Crystal growth, optical spectroscopy and laser action of Tm³⁺-doped monoclinic magnesium tungstate

LIZHEN ZHANG,[1] HAIFENG LIN,[1] GE ZHANG,[1] XAVIER MATEOS,[2,3] JOSEP M. SERRES,[2] MAGDALENA AGUILÓ,[2] FRANCESC DÍAZ,[2] UWE GRIEBNER,[3] VALENTIN PETROV,[3] YICHENG WANG,[3] PAVEL LOIKO,[4] ELENA VILEJSHIKOVA,[5] KONSTANTIN YUMASHEV,[5] ZHOUBIN LIN,[1,6] AND WEIDONG CHEN[1,3,*]

[1]*Key Laboratory of Optoelectronic Materials Chemistry and Physics, Fujian Institute of Research on the Structure of Matter, Chinese Academy of Sciences, Fuzhou, 350002 Fujian, China*
[2]*Física i Cristal·lografia de Materials I Nanomaterials (FiCMA-FiCNA), Universitat Rovira i Virgili (URV), Campus Sescelades, c/Marcel·lí Domingo, s/n., E-43007 Tarragona, Spain*
[3]*Max-Born-Institute for Nonlinear Optics and Ultrafast Spectroscopy, 2A Max-Born-Str., D-12489 Berlin, Germany*
[4]*ITMO University, 49 Kronverkskiy pr., 197101 St. Petersburg, Russia*
[5]*Center for Optical Materials and Technologies (COMT), Belarusian National Technical University, 65/17 Nezavisimosti Ave., 220013 Minsk, Belarus*
[6]*lzb@fjirsm.ac.cn*
[*]chenweidong@fjirsm.ac.cn

Abstract: We report on the crystal growth, spectroscopic investigation and laser performance of Tm³⁺-doped monoclinic magnesium tungstate (Tm:MgWO₄), for the first time, to the best of our knowledge. A high-quality crystal has been grown by the top seeded solution growth method. The relevant spectroscopic properties are characterized in terms of absorption, luminescence and Raman spectroscopy. Judd-Ofelt (J-O) analysis is performed to evaluate the spontaneous emission probabilities and the radiative lifetimes. The absorption, stimulated-emission and gain cross-section spectra are determined for the principal light polarizations. The first laser action in the 2 μm spectral range is demonstrated in the regime of continuous-wave operation with a maximum output power of 775 mW and a slope efficiency of 39%.

References and links

1. D. Theisen, V. Ott, H. W. Bernd, V. Danicke, R. Keller, and R. Brinkmann, "Cw high power IR-laser at 2 μm for minimally invasive surgery," Proc. SPIE **5142**, 96–100 (2003).
2. R. Targ, B. C. Steakley, J. G. Hawley, L. L. Ames, P. Forney, D. Swanson, R. Stone, R. G. Otto, V. Zarifis, P. Brockman, R. S. Calloway, S. H. Klein, and P. A. Robinson, "Coherent lidar airborne wind sensor II: flight-test results at 2 and 10 μm," Appl. Opt. **35**(36), 7117–7127 (1996).
3. V. Petrov, "Frequency down-conversion of solid-state laser sources to the mid-infrared spectral range using non-oxide nonlinear crystals," Progr. Quant. Electron. **42**, 1–106 (2015).
4. P. Loiko, J. M. Serres, X. Mateos, K. Yumashev, N. Kuleshov, V. Petrov, U. Griebner, M. Aguilo, and F. Diaz, "In-band-pumped Ho:KLu(WO₄)₂ microchip laser with 84% slope efficiency," Opt. Lett. **40**(3), 344–347 (2015).
5. V. Petrov, F. Guell, J. Massons, J. Gavalda, R. M. Sole, M. Aguilo, F. Diaz, and U. Griebner, "Efficient tunable laser operation of Tm:KGd(WO₄)₂ in the continuous-wave regime at room temperature," IEEE J. Quantum Electron. **40**(9), 1244–1251 (2004).
6. M. S. Gaponenko, P. A. Loiko, N. V. Gusakova, K. V. Yumashev, N. V. Kuleshov, and A. A. Pavlyuk, "Thermal lensing and microchip laser performance of N_g-cut Tm³⁺:KY(WO₄)₂ crystal," Appl. Phys. B **108**(3), 603–607 (2012).
7. V. Petrov, M. C. Pujol, X. Mateos, O. Silvestre, S. Rivier, M. Aguilo, R. M. Sole, J. H. Liu, U. Griebner, and F. Diaz, "Growth and properties of KLu(WO₄)₂, and novel ytterbium and thulium lasers based on this monoclinic crystalline host," Laser Photon. Rev. **1**(2), 179–212 (2007).

8. J. M. Cano-Torres, M. Rico, X. Han, M. D. Serrano, C. Cascales, C. Zaldo, V. Petrov, U. Griebner, X. Mateos, P. Koopmann, and C. Kränkel, "Comparative study of crystallographic, spectroscopic, and laser properties of Tm^{3+} in $NaT(WO_4)_2$ (T = La, Gd, Y, and Lu) disordered single crystals," Phys. Rev. B **84**(17), 174207-1–15 (2011).

9. E. Cavalli, A. Belletti, and M. G. Brik, "Optical spectra and energy levels of the Cr^{3+} ions in MWO_4 (M = Mg, Zn, Cd) and $MgMoO_4$ crystals," J. Phys. Chem. Solids **69**(1), 29–34 (2008).

10. V. B. Kravchenko, "Crystal structure of the monoclinic form of magnesium tungstate $MgWO_4$," J. Struct. Chem. **10**(1), 139–140 (1969).

11. V. B. Mikhailik, H. Kraus, V. Kapustyanyk, M. Panasyuk, P. Yu, V. Tsybulskyi, and L. Vasylechko, "Structure, luminescence and scintillation properties of the $MgWO_4$–$MgMoO_4$ system," J. Phys.: Cond. Matter **20**(36), 365219-1–8 (2008).

12. F. A. Danevich, D. M. Chernyak, A. M. Dubovik, B. V. Grinyov, S. Henry, H. Kraus, V. M. Kudovbenko, V. B. Mikhailik, L. L. Nagornaya, R. B. Podviyanuk, O. G. Polischuk, I. A. Tupitsyna, and Y. Y. Vostretsov, "$MgWO_4$ – A new crystal scintillator," Nucl. Instrum. Meth. A **608**(1), 107–115 (2009).

13. L. Li, Y. Yu, G. Wang, L. Zhang, and Z. Lin, "Crystal growth, spectral properties and crystal field analysis of Cr^{3+}:$MgWO_4$," Cryst. Eng. Comm. **15**(30), 6083–6089 (2013).

14. L. Zhang, Y. Huang, S. Sun, F. Yuan, Z. Lin, and G. Wang, "Thermal and spectral characterization of Cr^{3+}:$MgWO_4$ – a promising tunable laser material," J. Lumin. **169,** Part A, 161–164 (2016).

15. L. Zhang, W. Chen, J. Lu, H. Lin, L. Li, G. Wang, G. Zhang, and Z. Lin, "Characterization of growth, optical properties, and laser performance of monoclinic Yb:$MgWO_4$ crystal," Opt. Mater. Express **6**(5), 1627–1634 (2016).

16. L. F. Johnson, "Optical maser characteristics of rare-earth ions in crystals," J. Appl. Phys. **34**(4), 897–909 (1963).

17. K. Nassau and G. M. Loiacono, "Calcium tungstate-III: Trivalent rare earth substitution," J. Phys. Chem. Solids **24**(12), 1503–1510 (1963).

18. A. Lupei, V. Lupei, C. Gheorghe, L. Gheorghe, and A. Achim, "Multicenter structure of the optical spectra and the charge-compensation mechanisms in Nd:$SrWO_4$ laser crystals," J. Appl. Phys. **104**(8), 083102-1–7 (2008).

19. B. R. Judd, "Optical absorption intensities of rare-earth ions," Phys. Rev. **127**(3), 750–761 (1962).

20. G. S. Ofelt, "Intensities of crystal spectra of rare-earth ions," J. Chem. Phys. **37**(3), 511–520 (1962).

21. B. M. Walsh, N. P. Barnes, and B. Di Bartolo, "Branching ratios, cross sections, and radiative lifetimes of rare earth ions in solids: Application to Tm^{3+} and Ho^{3+} ions in $LiYF_4$," J. Appl. Phys. **83**(5), 2772–2787 (1998).

22. C. M. Dodson and R. Zia, "Magnetic dipole and electric quadrupole transitions in the trivalent lanthanide series: Calculated emission rates and oscillator strengths," Phys. Rev. B **86**(12), 125102-1–10 (2012).

23. A. S. Yasyukevich, V. G. Shcherbitskii, V. E. Kisel', A. V. Mandrik, and N. V. Kuleshov, "Integral method of reciprocity in the spectroscopy of laser crystals with impurity centers," J. Appl. Spectrosc. **71**(2), 202–208 (2004).

24. A. A. Kaminskii, H. J. Eichler, K. Ueda, N. V. Klassen, B. S. Redkin, L. E. Li, J. Findeisen, D. Jaque, J. García-Sole, J. Fernández, and R. Balda, "Properties of Nd^{3+}-doped and undoped tetragonal $PbWO_4$, $NaY(WO_4)_2$, $CaWO_4$, and undoped monoclinic $ZnWO_4$ and $CdWO_4$ as laser-active and stimulated Raman scattering-active crystals," Appl. Opt. **38**(21), 4533–4547 (1999).

25. P. Loiko, X. Mateos, S. Y. Choi, F. Rotermund, J. M. Serres, M. Aguiló, F. Díaz, K. Yumashev, U. Griebner, and V. Petrov, "Vibronic thulium laser at 2131 nm Q-switched by single-walled carbon nanotubes," J. Opt. Soc. Am. B **33**(11), D19–D27 (2016).

26. M. Segura, X. Mateos, M. C. Pujol, J. J. Carvajal, M. Aguilo, F. Diaz, U. Griebner, and V. Petrov, "Diode-pumped 2 μm vibronic (Tm^{3+}, Yb^{3+}):$KLu(WO_4)_2$ laser," Appl. Opt. **51**(14), 2701–2705 (2012).

27. M. N. Iliev, M. M. Gospodinov, and A. P. Litvinchuk, "Raman spectroscopy of $MnWO_4$," Phys. Rev. B **80**(21), 212302-1–4 (2009).

28. H. Wang, F. D. Medina, Y. D. Zhou, and Q. N. Zhang, "Temperature dependence of the polarized Raman spectra of $ZnWO_4$ single crystals," Phys. Rev. B **45**(18), 10356–10362 (1992).

1. Introduction

Laser gain media doped with Tm are of great interest for obtaining coherent radiation around 2 μm due to the $^3F_4 \rightarrow {}^3H_6$ transition of the Tm^{3+} ion. The emission of Tm-based lasers is "eye-safe" and it matches spectrally the strong absorption bands of such molecules as H_2O, NO_2, CO_2 and NH_3. Already established applications of Tm lasers include medical surgery [1], remote atmospheric sensing [2] and pumping of mid-infrared optical parametric oscillators (OPOs) [3] or holmium (Ho^{3+}) based lasers [4].

Double tungstate crystals represent an important class of laser host materials and they were extensively investigated with Tm^{3+} doping in the regimes of continuous-wave (CW) operation, Q-switching, and mode-locking. The most profound examples are the ordered Tm^{3+}-doped monoclinic potassium (rare-earth) double tungstates $KRE(WO_4)_2$ where RE = Gd [5], Y [6] or

Lu [7], and the disordered tetragonal sodium double tungstates $NaRE(WO_4)_2$ where RE = Gd, Y, Lu or La [8]). The title compound, magnesium tungstate ($MgWO_4$) belongs to another crystal family of monoclinic (sp. gr. *P2/c*) divalent metal monotungstates, having the general chemical formula MWO_4 where M = Mg, Mn, Ni, Cd or Zn [9,10]. Earlier investigations of $MgWO_4$ focused on its application as scintillator [11,12]. Only very recently, $MgWO_4$ attracted attention as a promising laser host for doping with transition-metal ions, e.g. Cr^{3+} [13,14], and RE ions, e.g. Yb^{3+} [15]. The difference in ionic radius between the divalent Mg^{2+} ion and trivalent RE ions induces distortion of the crystal field, which leads to broadening of the absorption and emission spectra [16-18]. This advantage is essential for broadly tunable laser operation and the generation of ultrashort pulses in the mode-locking regime. The monoclinic $MgWO_4$ crystal is optically biaxial, thus polarization anisotropy of the spectroscopic properties of the RE dopant can be expected, leading to naturally polarized laser output. The thermal conductivity of the $MgWO_4$ host crystal measured for unknown orientation is ~8.7 W/mK or almost 3 times larger than that of double tungstate crystals [14].

Recently, we have demonstrated efficient laser operation with Yb^{3+}-doped $MgWO_4$ crystal [15]. Motivated by this success and the diversity of applications of 2 μm laser sources, we extended this work aiming to develop a high quality $MgWO_4$ crystal with Tm^{3+} doping. In the present work, we report on the crystal growth, spectroscopy and CW laser operation of monoclinic $Tm:MgWO_4$ crystal, for the first time to the best of our knowledge.

2. Crystal growth

The $Tm:MgWO_4$ crystal was grown by the top-seeded solution growth (TSSG) method with a flux of Na_2WO_4 in a vertical tubular furnace. The ratio of $MgWO_4:Na_2WO_4$ in the melt was 5:7 (mol). The powder precursors were Na_2CO_3, MgO and WO_3 with analytical grade of purity, and Tm_2O_3 with a purity of 99.99%. Stoichiometric amounts of raw materials with 10 at.% Tm_2O_3 were prepared by repeated solid state reactions. The mixtures of solute and flux were placed into a platinum crucible and sintered in a resistance furnace at 970 °C for 48 h. The crystal was grown at a cooling rate of 0.5–0.8°C/day and rotation rate of 10–15 rpm. The details of the furnace and parameters of the temperature controlling program can be found elsewhere [13,15]. The bulk $Tm:MgWO_4$ crystal finally obtained had dimensions of $16 \times 8 \times 6$ mm³, as shown in Fig. 1(a). The as-grown crystal had a yellowish coloration which originated from optical absorption in the 320–420 nm spectral range. This absorption is observed in undoped crystals as well as it is attributed to color centers [12,15].
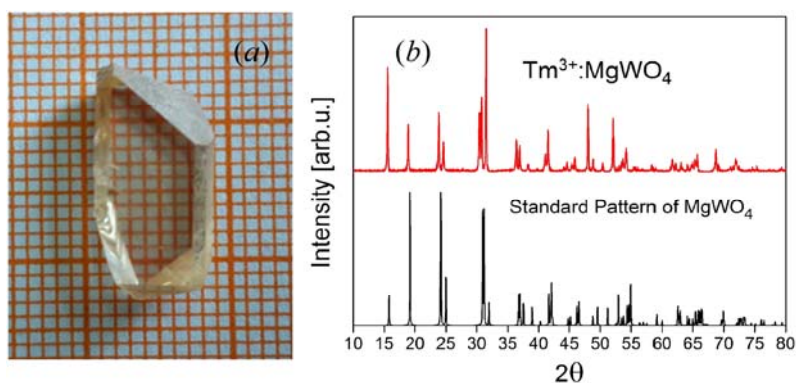

Fig. 1. (a) Photograph of the as-grown $Tm:MgWO_4$ boule; (b) X-ray diffraction pattern of the powdered as-grown $Tm:MgWO_4$ crystal.

To confirm the symmetry of the as-grown crystal, the X-ray powder diffraction (XRD) pattern was measured at room temperature by using a desktop X-ray diffractometer (Rigaku, MiniFlex 600) equipped with Cu Kα radiation. The experiment was carried out in the $2\theta = 10$–

80° range with a step of 0.02° and a scan speed of 0.13°/min. Figure 1(b) shows the XRD pattern of a powdered as-grown crystal. The diffraction peaks are consistent with the standard pattern of undoped $MgWO_4$ (crystallographic database, powder diffraction file #27-0789 for Huanzalaite). $MgWO_4$ belongs to the monoclinic crystal class (point group $2/m$, space group $P2/c$). Based on the XRD analysis, the lattice constants of Tm:$MgWO_4$ are a = 4.697 Å, b = 5.678 Å, c = 4.933 Å, $\beta = a{\wedge}c$ = 90.77° (V = 131.54 Å^3, Z = 2). They are larger than those of the undoped crystal (a = 4.686 Å, b = 5.675 Å, c = 4.928 Å, $\beta = a{\wedge}c$ = 90.3° [12]). This is attributed to the different ionic radii of Tm^{3+} and Mg^{2+} (0.88 and 0.72 Å, respectively, for the VI-fold O^{2-}–coordination). The calculated crystal density of Tm:$MgWO_4$ is 6.871 g/cm^3.

The concentration of Tm^{3+} ions in the as-grown crystal was determined to be 0.89 at.%, i.e. $1.409{\times}10^{20}$ at/cm^3 by using the Inductively Coupled Plasma Atomic Emission Spectrometry (ICP-AES) method. The calculated segregation coefficient of the Tm^{3+} ion is K_{Tm} = 0.09.

3. Spectroscopic characterization

Monoclinic crystals are optically biaxial and their optical properties are described in the frame of the optical indicatrix with three mutually orthogonal principal axes X, Y and Z. Since the refractive indices of $MgWO_4$ are still unknown, following [15] we have arbitrarily chosen the Y-axis to be parallel to the crystallographic *b*-axis which coincides with the 2-fold symmetry axis. The other two axes of the optical indicatrix, namely X and Z, are located in the *a-c* plane. The rotation of the optical indicatrix relative to the crystallographic frame is expressed by the angles $a{\wedge}X$ = 36.4° and $c{\wedge}Z$ = 37.1° [15]. We have studied all the spectroscopic properties of Tm^{3+} in $MgWO_4$ for the principal light polarizations E || X, Y and Z at room-temperature (RT, 293 K).

3.1 Optical absorption

In order to evaluate the optimum pump conditions for Tm:$MgWO_4$ and to calculate the absorption and stimulated emission cross-sections, polarized absorption measurements were carried out in the 0.3–2.1 μm spectral range, Fig. 2(a). Tm^{3+} ions in $MgWO_4$ exhibit strong anisotropy of the optical absorption. The observed absorption bands are assigned to the transitions from the $^3H_6$ ground state of Tm^{3+} to the excited states $^1G_4$, $^3F_{2,3}$, $^3H_4$, $^3H_5$, and $^3F_4$.
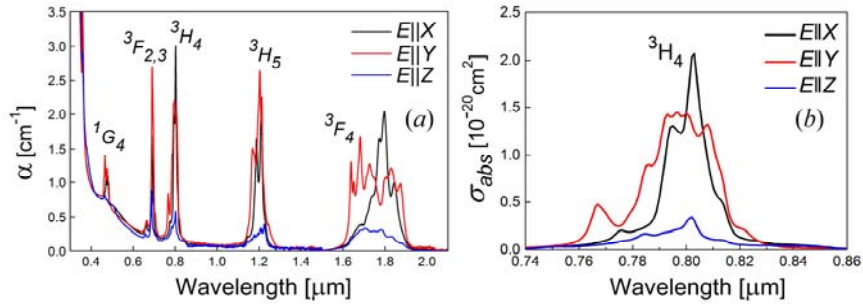

Fig. 2. (a) RT polarized absorption of 0.89 at.% Tm:$MgWO_4$, α is the absorption coefficient; (b) RT absorption cross-section, σ_{abs}, spectra corresponding to the $^3H_6 \rightarrow {}^3H_4$ transition.

The band related to the $^3H_6 \rightarrow {}^3H_4$ transition is suitable for pumping of Tm:$MgWO_4$ with commercially available AlGaAs diode lasers emitting around 800 nm. The corresponding polarized absorption cross-sections, σ_{abs}, are shown in Fig. 2(b); they were calculated from the measured absorption coefficient as $\sigma_{abs} = \alpha/N_{Tm}$. The maximum σ_{abs} is $2.04{\times}10^{-20}$ cm^2 at 802.6 nm for light polarization E || X and the full width at half maximum (FWHM) of this peak is ~14 nm. For E || Y, σ_{abs} = $1.45{\times}10^{-20}$ cm^2 at 796.4 nm with FWHM = 31 nm and for E || Z, σ_{abs} = $0.34{\times}10^{-20}$ cm^2 at 801.8 nm with FWHM = 25 nm. The absorption linewidths of Tm:$MgWO_4$ around 800 nm are much broader compared to the most intensively studied Tm^{3+}-

doped laser crystals, YAG and YLF, and broader than in the monoclinic double tungstates $KRE(WO_4)_2$ where RE = Gd, Y or Lu [5-7]. This relaxes the requirements for wavelength stabilization of the AlGaAs diode lasers acting as a pump source. We attribute this broadening of the spectral bands to the distortion of the crystal field symmetry when the Tm^{3+} ions are replacing the Mg^{2+} ones in the $MgWO_4$ lattice [16-18].

The absorption spectra of Tm^{3+} in $MgWO_4$ were analyzed in the frame of the standard Judd-Ofelt (J-O) theory [19,20] in order to determine the spontaneous emission probabilities. The absorption oscillator strengths were determined from the measured absorption spectra:

$$f_{\exp}(JJ') = \frac{m_e c^2}{\pi e^2 N_{Tm} \langle \lambda \rangle^2} \Gamma(JJ'), \tag{1}$$

where m_e and e are the electron mass and charge, respectively, c is the speed of light, $\Gamma(JJ')$ is the integrated absorption coefficient within the absorption band and $\langle \lambda \rangle$ is the "center of gravity" of the absorption band. The experimental absorption oscillator strengths were averaged over the principal light polarizations, $1/3 \times (f_X + f_Y + f_Z)$. The results are shown in Table 1.

The values of $f_{\exp}$ were used to determine the J-O (intensity) parameters, Ω_k, $k = 2, 4, 6$. For $Tm:MgWO_4$, they are $\Omega_2 = 7.609$, $\Omega_4 = 0.841$ and $\Omega_6 = 2.376$ [10^{-20} cm^2]. With these parameters, the absorption oscillator strengths f were calculated, showing a good agreement with the experiment:

$$f_{calc}(JJ') = \frac{8}{3h(2J'+1)\langle \lambda \rangle} \frac{(n^2+2)^2}{9n} S_{calc}(JJ') + f_{MD}(JJ'), \tag{2a}$$

$$S_{calc}(JJ') = \sum_{k=2,4,6} U^{(k)} \Omega_k, \text{where } U^{(k)} = \langle (4f^n)SLJ \| U^k \| (4f^n)S'L'J' \rangle^2. \tag{2b}$$

Here, S_{calc} are the line strengths, h is the Planck constant, n is the refractive index of the crystal and $U^{(k)}$ are the squared reduced matrix elements [21]. J-O theory describes electric-dipole (ED) transitions. The contribution of magnetic-dipole (MD) transitions with J–J' = 0, ± 1, f_{MD}, was taken from the literature [22].

Table 1. Experimental and Calculated Absorption Oscillator Strengths for Tm:MgWO₄ Crystal

Transition	$\langle \lambda \rangle$, nm	$\langle E \rangle$, cm^{-1}	$U^{(2)}$	$U^{(4)}$	$U^{(6)}$	Γ, cm^{-1}nm	$f_{\exp} \times 10^6$	$f_{calc} \times 10^6$
$^3H_6 \rightarrow ^3F_4$	1759	5684	0.537	0.726	0.238	175.2	4.57	4.60^{ED}
$^3H_6 \rightarrow ^3H_5$	1196	8359	0.107	0.231	0.638	70.2	3.96	3.25^{ED}+0.52^{MD}
$^3H_6 \rightarrow ^3H_4$	797.5	12539	0.237	0.109	0.595	49.6	6.29	6.37^{ED}
$^3H_6 \rightarrow ^3F_3$	689.1	14513	0	0.316	0.841	28.7	4.87	5.05^{ED}
$^3H_6 \rightarrow ^1G_4$	480.5	20813	0.048	0.075	0.013	6.5	2.28	1.47^{ED}

$\langle \lambda \rangle$ - "center of gravity" of the absorption band, $\langle E \rangle$ – the corresponding estimated energy of the multiplet barycenter, $U^{(k)}$, $k = 2, 4, 6$ – squared reduced matrix elements, Γ – integrated absorption coefficient, $f_{\exp}$ and f_{calc} – experimental and calculated absorption oscillator strengths, respectively. ED and MD stand for the electric-dipole and magnetic-dipole contributions, respectively.

3.2 Luminescence (emission and lifetime)

The photoluminescence (PL) of Tm^{3+} in $MgWO_4$ was characterized in terms of emission spectra and lifetime. The normalized polarized PL spectra were measured in the 1.3–2.1 μm spectral range under excitation at 802 nm, see Fig. 3. There are two bands in the spectra which correspond to the $^3H_4 \rightarrow ^3F_4$ and $^3F_4 \rightarrow ^3H_6$ transitions, respectively. Note that the PL spectra also exhibits strong polarization anisotropy.

The probabilities of spontaneous radiative transitions were calculated from the corresponding line strengths which, in turn, were derived from the J-O parameters Ω_k and squared reduced matrix elements $U^{(t)}$, see Eq. (2b):

$$A_{calc}(JJ') = \frac{64\pi^4 e^2}{3h(2J'+1)\langle\lambda\rangle^3} n\left(\frac{n^2+2}{3}\right)^2 S_{ED}^{calc}(JJ') + A_{MD}(JJ').$$ (3)

The MD contributions A_{MD} were taken from the literature [22]. On the basis of probabilities of spontaneous transitions for the separate emission channels J→J', we have calculated the total probability, A_{tot}, the corresponding radiative lifetime of the excited-state, τ_{rad}, and the luminescence branching ratios for the emission channels, $B(JJ')$:

$$\tau_{rad} = \frac{1}{A_{tot}}, \text{ where } A_{tot} = \sum_{J'} A_{calc}(JJ'),$$ (4a)

$$B(JJ') = \frac{A_{calc}(JJ')}{\sum_{J'} A_{calc}(JJ')}.$$ (4b)

The results are summarized in Table 2. In particular, the radiative lifetime of the lowest excited-state, $\tau_{rad}(^3F_4) = 1.95$ ms.
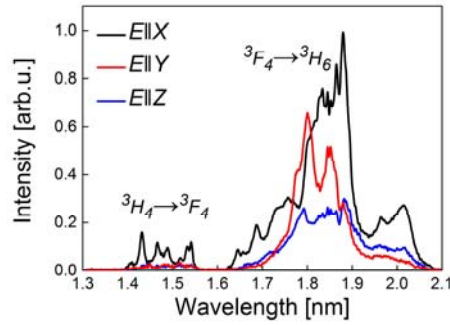

Fig. 3. Normalized RT photoluminescence spectra of Tm:MgWO$_4$ under 802 nm excitation for light polarizations E || X, Y and Z.

Table 2. Calculated Emission Probabilities for Tm^{3+} in MgWO$_4$

Excited state	Final state	$\langle\lambda\rangle$, nm	$U^{(2)}$	$U^{(4)}$	$U^{(6)}$	$A_{JJ'}$, s^{-1}	$B_{JJ'}$, %	A_{tot}, s^{-1}	τ_{rad}, ms
$^3F_4$	$^3H_6$	1759	0.537	0.726	0.238	514.1^{ED}	1	514.1	1.95
$^3H_5$	$^3F_4$	3740	0.091	0.128	0.928	25.1^{ED}+1.4^{MD}	3.4	770.0	1.30
	$^3H_6$	1196	0.107	0.231	0.638	645.4^{ED}+98.0^{MD}	96.6		
$^3H_4$	$^3H_5$	2392	0.013	0.479	0.009	20.4^{ED}+12.4^{MD}	0.9	3817	0.26
	$^3F_4$	1459	0.129	0.130	0.206	271.9^{ED}+27.5^{MD}	7.8		
	$^3H_6$	797.5	0.237	0.109	0.595	3485^{ED}	91.3		
$^3F_3+^3F_2$	$^3H_4$	5066	0.082	0.354	0.285	9.9^{ED}+0.3^{MD}	0.2	5625	0.17
	$^3H_5$	1625	0.629	0.346	0	823.8^{ED}	14.6		
	$^3F_4$	1133	0.003	0.001	0.167	217.3^{ED}+68.6^{MD}	5.1		
	$^3H_6$	689.0	0	0.316	0.850	4505^{ED}	80.1		
$^1G_4$	$^3F_2$	1735	0.006	0.072	0.041	21.1^{ED}	0.4	5494	0.18
	$^3F_3$	1587	0.010	0.071	0.230	113.5^{ED}+4.1^{MD}	2.1		
	$^3H_4$	1209	0.156	0.004	0.370	626.5^{ED}+39.5^{MD}	12.1		
	$^3H_5$	803.0	0.073	0.005	0.536	1888^{ED}+177.7^{MD}	37.6		
	$^3F_4$	661.0	0.004	0.020	0.072	397.0^{ED}+10.6^{MD}	7.4		
	$^3H_6$	480.5	0.048	0.075	0.013	2216^{ED}	40.3		

$\langle\lambda\rangle$ - mean wavelength of the emission band, $U^{(k)}$, k = 2, 4, 6 – squared reduced matrix elements, $A_{JJ'}$ – probability of radiative spontaneous transition, $B_{JJ'}$ – luminescence branching ratio, A_{tot} and τ_{rad} – total probability of radiative spontaneous transitions and the radiative lifetime of the excited state, respectively. ED and MD stand for the electric-dipole and magnetic-dipole contributions, respectively.

The stimulated emission, σ_e, cross-section spectra for the $^3F_4 \rightarrow {}^3H_6$ transition of Tm^{3+} in $MgWO_4$ were calculated from the measured absorption spectra by using the modified reciprocity method [23]:

$$\sigma_e^i(\lambda) = \frac{1}{8\pi n^2 \tau_{rad} c} \frac{3\sigma_{abs}^i(\lambda)\exp(-hc/(kT\lambda))}{\sum\limits_{i=X,Y,Z} \int \lambda^{-4}\sigma_{abs}^i(\lambda)\exp(-hc/(kT\lambda))d\lambda}. \tag{5}$$

Here, σ_e^i and σ_{abs}^i (i = X, Y or Z) are the stimulated-emission and absorption cross-sections for the i-th principal light polarization, k is the Boltzmann constant, T is the temperature, τ_{rad} is the radiative lifetime of the emitting state ($^3F_4$ state of Tm^{3+}). The results for σ_{abs} and σ_e for Tm:MgWO$_4$ are presented in Fig. 4. The maximum σ_e is 2.43×10^{-20} cm^2 at 1877 nm for light polarization $\boldsymbol{E} \parallel$ Y. For $\boldsymbol{E} \parallel$ X, the emission band contains two local peaks at 1799.5 and 1848.5 nm with $\sigma_e \sim 1.63 \times 10^{-20}$ cm^2. The maximum σ_e for $\boldsymbol{E} \parallel$ Z polarization is 0.32×10^{-20} cm^2 at 1884 nm. These emission cross-sections are comparable to the monoclinic double tungstates but much higher compared to the commonly used Tm^{3+}-doped YAG and YLF crystals [5]. The anisotropy of the maximum stimulated emission cross-sections, $\sigma_e(X)$: $\sigma_e(Y)$: $\sigma_e(Z)$, amounts to 5.1:7.6:1. Note that such a pronounced anisotropy will promote natural polarization selection and linearly polarized output from a Tm:MgWO$_4$ laser.
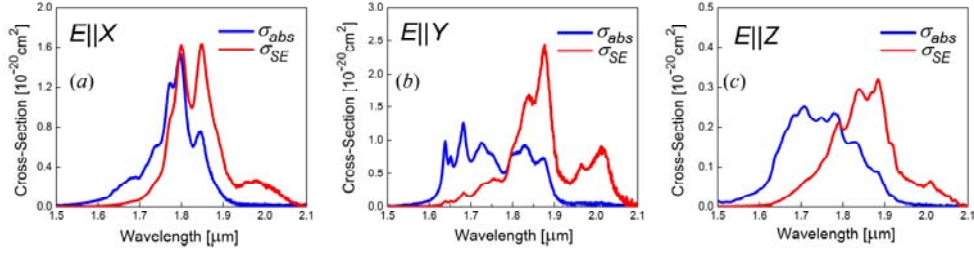

Fig. 4 (a)-(c) RT absorption (σ_{abs}) and stimulated-emission (σ_e) cross-section spectra for the $^3H_6 \leftrightarrow {}^3F_4$ transition of Tm^{3+} in MgWO$_4$ for light polarizations $\boldsymbol{E} \parallel$ X (a), $\boldsymbol{E} \parallel$ Y (b) and $\boldsymbol{E} \parallel$ Z (c). The σ_e spectra are derived with the modified reciprocity method.

The luminescence lifetime τ_{lum} of the $^3F_4$ state of Tm^{3+} in MgWO$_4$ was determined by a decay measurement. The sample was powdered in order to eliminate the effect of radiation trapping. By exciting the Tm^{3+} ions at 802 nm, we monitored the luminescence decay at ~1850 nm (from the $^3F_4$ excited state). The results are presented in Fig. 5. The decay is clearly single-exponential and the dependence was fitted by τ_{lum} = 1.93 ms. The luminescence lifetime of the $^3F_4$ state is very close to the radiative one determined from the J-O calculation. Therefore, the luminescence quantum yield $\eta_q = \tau_{lum}/\tau_{rad} > 99\%$ which indicates very weak non-radiative relaxation from this state. This is a consequence of the large energy-gap to the ground-state but also indicates very good optical quality of the as-grown crystal.
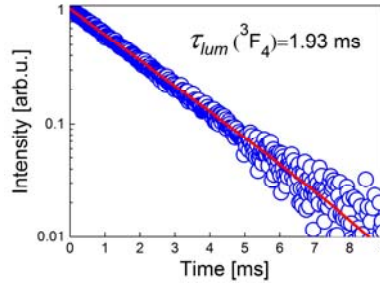

Fig. 5. Decay curve of the Tm^{3+} luminescence from the $^3F_4$ state for a 0.89 at.% Tm:MgWO$_4$ crystal: *symbols* –experimental data, *solid line* - single-exponential fit, excitation wavelength – 802 nm, emission wavelength – 1850 nm.

The laser emission range for Tm:MgWO$_4$ can be predicted from the corresponding gain cross-section, σ_{gain}, spectra. Here, $\sigma_{gain} = \beta\sigma_e - (1-\beta)\sigma_{abs}$, $\beta = N(^3F_4)/N_{Tm}$ represents the inversion ratio, i.e. the number of the Tm^{3+} ions in the excited state $N(^3F_4)$ divided by the total ion density N_{Tm}. The σ_{gain} spectra for the $^3F_4 \rightarrow {}^3H_6$ transition of Tm^{3+} in MgWO$_4$ are shown in Fig. 6 for the three principal light polarizations $\boldsymbol{E} \parallel$ X, Y and Z.
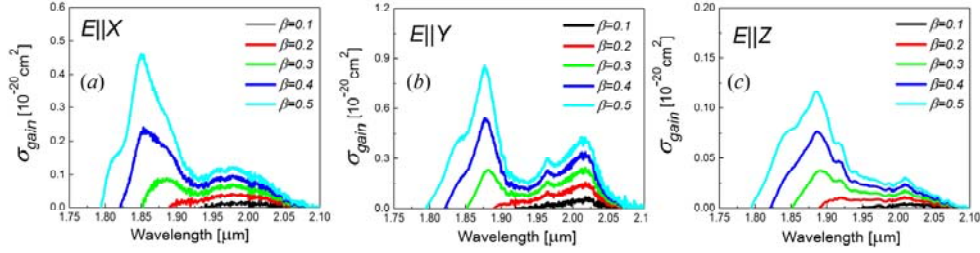
Fig. 6 (a)-(c). Gain cross-section $\sigma_{gain} = \beta\sigma_e - (1-\beta)\sigma_{abs}$ for the $^3F_4 \rightarrow {}^3H_6$ transition of Tm^{3+} in MgWO$_4$ and light polarization $\boldsymbol{E} \parallel$ X (a), $\boldsymbol{E} \parallel$ Y (b) and $\boldsymbol{E} \parallel$ Z (c), $\beta = N(^3F_4)/N_{Tm}$ is the inversion ratio.

The maximum gain cross-sections correspond to light polarization $\boldsymbol{E} \parallel$ Y. Thus, one may expect laser oscillation with this polarization for X-cut and Z-cut Tm:MgWO$_4$ crystals. For low inversion ratios ($\beta < 0.3$), the local peak centered at ~2.02 μm dominates in the spectrum. For higher β, one may expect a jump of the emission wavelength to ~ 1.88 μm or even a dual-wavelength operation. For high inversion levels, one may expect tuning of the laser emission in the 1.85–2.06 μm range (i.e., >200 nm tunability). For Y-cut Tm:MgWO$_4$, the laser will most probably operate in the $\boldsymbol{E} \parallel$ X polarization. In the corresponding gain spectra, the position of the local peaks is at ~1.98 μm (for $\beta < 0.2$) and at 1.85 μm (for higher β).

3.3 Raman spectra

Mono- and double tungstate crystals are well-known for their Raman activity. Undoped crystals are used as Raman shifters [24] for sub-ns and ps pulses while RE-doped ones are used for self-Raman conversion in Q-switched and CW lasers. Recently, Tm^{3+}-doped monoclinic double tungstates were found to be very suitable for vibronic laser operation relying on electron-phonon coupling with the low-energy Raman–active vibrational modes [25,26]. From this point of view, the study of the Raman spectra of the monoclinic Tm:MgWO$_4$ crystal is of high interest for laser applications.

Polarized Raman spectra of Tm:MgWO$_4$ were measured at room temperature, see Fig. 7(a-c). Here, we use standard notations $a(bc)d$, where a and d correspond to the directions of propagation of incident and scattered light, and b and c – to their polarizations, respectively. The cases $a = d =$ X, Y or Z are considered. The group analysis of the MgWO$_4$ structure predicts 36 lattice modes of which 18 even (g) vibrations are Raman-active: $8A_g+10B_g$, see Table 3. For the WO$_6$ octahedra, there are 6 active modes related to 6 W-O bonds: $4A_g+2B_g$. Typically, the internal vibrations of a tightly bound group of atoms have higher frequencies and can easily be assigned. An example is the scheelite structure, CaWO$_4$, with two sets of modes at 0-409 and 797-912 cm^{-1} (the latter being internal). For MgWO$_4$, the WO$_6$ octahedra share two oxygen atoms and the ranges of external/internal modes may overlap. The internal modes are marked in Table 3 by asterisk, following [27,28]. The most intense mode at 916 cm^{-1} (FWHM = 13.6 cm^{-1}) is assigned to the symmetric stretching W-O vibrations A_{1g}, the modes at 812 and 709 cm^{-1} – to the asymmetric stretching E_g, and the modes at 683, 551 and 420 cm^{-1} – to the bending (T_g) of the regular octahedron. The remaining modes are external and they are related to the interaction of the WO$_6$ groups with Mg atoms through the Mg-W, Mg-W-O and Mg-WOOW vibrations.
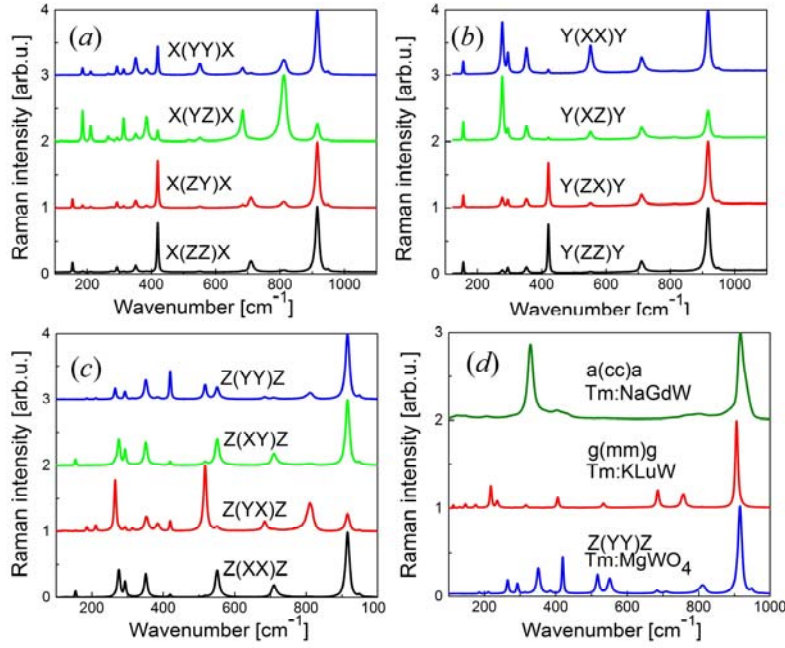
Fig. 7 (a)-(c). Polarized Raman spectra of the Tm:MgWO$_4$ crystal for X(_)X (a), Y(_)Y (b) and Z(_)Z (c) geometries (the excitation wavelength is 514 nm) and (d) comparison of the Raman spectra of Tm:MgWO$_4$, Tm:KLu(WO$_4$)$_2$ (KLuW) and Tm:NaGd(WO$_4$)$_2$ (NaGdW) crystals.

Table 3. Raman-Active Modes Observed in Tm:MgWO$_4$

Mode	v, cm^{-1}	Symmetry	Assignment	Mode	v, cm^{-1}	Symmetry
1*	916	A_g	$v_1(A_{1g})$	10	313	B_g
2*	812	B_g	$v_2(E_g)$	11	276	A_g
3*	709	A_g	$v_2(E_g)$	12	262	B_g
4*	683	B_g	$v_3(T_g)$	13	211	A_g
5*	551	A_g	$v_3(T_g)$	14	186	B_g
6	517	B_g		15	154	B_g
7*	420	A_g	$v_3(T_g)$	16	134	B_g
8	384	B_g		17	121	A_g
9	352	A_g		18	98	B_g

*Internal modes.

In Fig. 7(d), we compare the Raman spectrum of Tm:MgWO$_4$ with those of two double tungstate crystals employed for Tm^{3+} doping: monoclinic KLu(WO$_4$)$_2$ and tetragonal scheelite-like NaGd(WO$_4$)$_2$. The spectra of the monoclinic crystals are similar due to the presence of double oxygen bridge vibrations. The appearance of low- and medium-energy modes for Tm:MgWO$_4$ at 150-550 cm^{-1} may provide efficient vibronic laser operation at 2.1~2.2 μm.

4. Continuous-wave laser performance

For the laser experiments, a sample from the as-grown crystal was cut for light propagation along the Z-axis with an aperture of 1.86(X)×3.96(Y) mm^2 and a thickness of 3.05 mm. Both X×Y crystal faces were polished to laser quality and remained uncoated. The laser crystal was mounted in a Cu-holder and Indium foil was used to provide improved thermal contact from all 4 lateral sides. The holder was water-cooled to 12°C. A hemispherical laser cavity was used. The pump mirror (PM) was antireflection (AR) coated at 0.77-1.05 μm and high reflection (HR) coated at 1.80-2.08 μm. It was located at 1 mm from the laser crystal.

Several concave output couplers (OCs) with radius of curvature of R_{OC} = 50 mm and transmission (T_{OC}) of 1%, 3%, 5% and 15% at the laser wavelength were employed. The total geometrical cavity length was ~49 mm. The laser crystal was pumped through the PM by a fiber-coupled laser diode (LD) at ~802 nm (fiber diameter: 200 μm, N.A. = 0.22). The unpolarized pump beam was re-imaged into the laser crystal by a lens assembly with a 1:1 imaging ratio. The pump spot size in the crystal was w_p = 100 μm (the beam propagation factor M^2 of the diode laser output was calculated to be 86, and the confocal parameter $2z_R$ was 1.9 mm). The single pass pump absorption of the crystal was 30%. The scheme of the $Tm:MgWO_4$ laser is shown in Fig. 8.
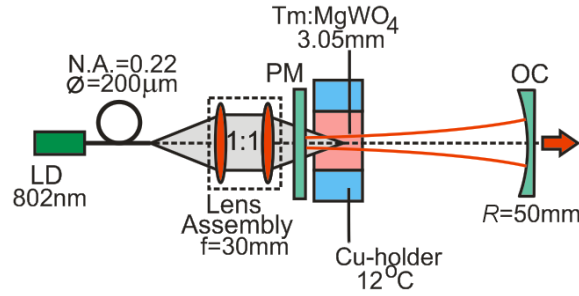
Fig. 8. Scheme of the $Tm:MgWO_4$ laser: LD – laser diode, PM – pump mirror, OC – output coupler.
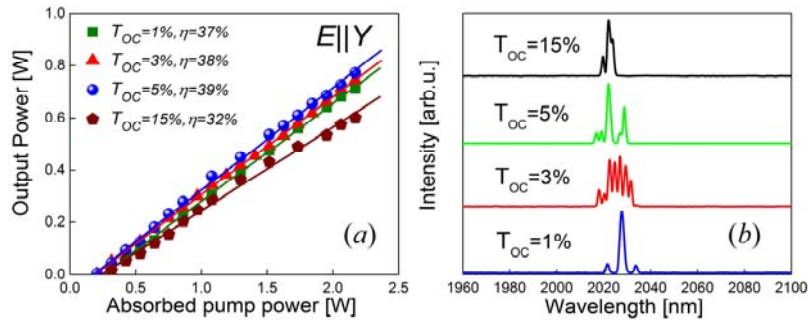
Fig. 9. CW $Tm:MgWO_4$ laser: (a) input-output dependences, η – slope efficiency; (b) typical laser emission spectra measured at P_{abs} = 2.17 W.

The input-output characteristics and the emission spectra of the $Tm:MgWO_4$ laser are presented in Fig. 9. For all the studied OCs, the laser emission was linearly polarized ($E \parallel$ Y); the polarization was naturally-selected by the anisotropy of the gain. No polarization-switching was detected. The output power dependence was clearly linear showing no detrimental influence of the thermal effects. The maximum output power was 772 mW at 2017-2029 nm (multi-peak spectrum) corresponding to a slope efficiency of η = 39% (with respect to the absorbed pump power), as measured with T_{OC} = 5%. The laser threshold was at P_{abs} = 0.19 W and the optical-to-optical efficiency η_{opt} was 11% (with respect to the incident pump power). For smaller T_{OC}, the laser performance was slightly inferior, resulting in decreased slope efficiency η = 38% (T_{OC} = 3%) and η = 37% (T_{OC} = 1%). For large T_{OC} = 15%, the output power dropped further which is attributed to the increased upconversion losses. The laser emission spectra were weakly dependent on the output coupling, see Fig. 9(b), and the emission occurred in the 2017-2034 nm spectral range in agreement with the gain spectra for light polarization $E \parallel$ Y.

5. Conclusion

In conclusion, we report on the growth of monoclinic Tm:MgWO$_4$ and its polarization-resolved spectroscopic characteristics and achieved for the first time laser operation with this new crystal. Absorption, stimulated-emission and gain cross-section spectra are obtained for the relevant transitions of the Tm^{3+} ion. Raman spectra are also measured. The Judd-Ofelt (J-O) analysis is performed to determine the spontaneous emission probabilities, luminescence branching ratios and radiative lifetimes. The luminescence of Tm^{3+} ions is characterized in terms of spectral and decay measurements. Laser operation of Tm in MgWO$_4$ is realized in a compact cavity in the CW regime under diode-pumping.

The spectroscopic features of Tm:MgWO$_4$ are determined by its low-symmetry structure and the distortion of the rare-earth site caused by the mismatch of the ionic radii of Mg^{2+} and Tm^{3+}. This provides a substantial broadening of the absorption and emission spectral bands, as well as strong polarization-anisotropy of the transition cross-sections. The polarizations of interest in Tm:MgWO$_4$ for reaching high pump efficiency and high gain are $E \parallel X$ and $E \parallel Y$. For these polarizations, Tm:MgWO$_4$ is promising for broad tuning of the laser emission (with expected tuning range of >200 nm) and generation of ultrashort pulses at wavelengths above 2 µm. The broad (FWHM ~20 nm) and intense absorption band related to the $^3H_6 \rightarrow {}^3H_4$ transition relaxes the requirements for wavelength stabilization of the AlGaAs laser diodes employed for Tm:MgWO$_4$ pumping. A relatively long lifetime (1.93 ms) of the upper laser level of Tm^{3+} in MgWO$_4$ makes this material very promising also for generation of high pulse energies in the Q-switched operation mode. Further increase of the slope efficiency of Tm:MgWO$_4$ lasers is possible for higher Tm doping levels by enhancing the efficiency of cross-relaxation for adjacent Tm^{3+} ions. MgWO$_4$ has a rich Raman spectrum which may be used for extending the emission range of Tm:MgWO$_4$ lasers to >2.1 µm with vibronic coupling. The codoping of MgWO$_4$ with Tm^{3+} and Ho^{3+} ions may also offer another alternative for such long-wavelength emission.